2024-01-2196 Published 09 Apr 2024

Stress Generation in Large Pouch Cells Under Cycling and Abuse Conditions

Andre Swarts, Swapnil Suryakant Salvi, and Travis Holmgreen Southwest Research Institute

Citation: Swarts, A., Salvi, S.S., and Holmgreen, T., "Stress Generation in Large Pouch Cells Under Cycling and Abuse Conditions," SAE Technical Paper 2024-01-2196, 2024, doi:10.4271/2024-01-2196.

Received: 08 Nov 2023 Revised: 25 Jan 2024 Accepted: 03 Feb 2024

Abstract

Pouch cells are increasingly popular form factors for the construction of energy storage systems in electric vehicles of all classes. Knowledge of the stress generated by these higher capacity pouch cells is critical to properly design battery modules and packs for both normal and abnormal operation. Existing literature predominantly offers data on smaller pouch cells with capacities of less than 10 Ah, leaving a gap in our understanding of the behavior of these larger cells. This experimental study aimed to bridge this knowledge gap by measuring loads and stresses in constrained 65 Ah pouch cells under both cycling and abuse conditions. To capture the desired responses, a load cell was located within a robust fixture to measure cell stress in real time after the application of a preload of approximately 30 kilograms or 294 N, equivalent to a pressure of 0.063 bar, with a fixed displacement. The thermal distribution across the cells was monitored by thermocouples at multiple locations. Cell voltage and current measurements were done concurrently and all data was recorded continuously using a dedicated data acquisition system, supplemented by video imagery and post-test cell inspections and photographs. A cycling test was conducted over multiple charge-discharge cycles at a C/3 rate to monitor the stress development associated with cell ageing. The results revealed an increase in the maximum load from about 2000 N (0.43 bar) to more than 4,200 N (0.91 bar) after 34 cycles. Additionally, two short-circuit abuse tests were performed with an external hard short, simulating a potential failure scenario. The first test revealed peak loads of approximately 800 N (0.71 bar) before an unplanned electrical disconnection terminated the test. The peak load for the second test exceeded 4,200 N (0.91 bar) and before loss of the electrolyte.

Introduction

Pouch cells are an increasingly popular form factor due to the high energy density, both volumetric and gravimetric, when deployed in energy storage systems, especially for electric vehicle applications. Much of this benefit comes from the fact that the cells have limited inherent structure, unlike cylindrical and prismatic cells, which require the pouch cells to be provided with support.

Pouch cells are typically deployed in closely packed modules, relying on conduction as the primary mode of heat transfer. Pairs of cells are often joined to a thermally conductive separator which is itself coupled to the cold plate with a thermal interface material (for example in the Ford Mustang Mach-E pack) or by direct thermal connection to the sides of the module (for example in the VW ID.3). Such a close packing provides the requisite structural support.

One further consequence of the lack of an inherent structure is dimensional changes, especially in the thickness of the cells, as a result of normal operation (charging and discharging), due to irreversible cell ageing. The reasons are varied and include the expansion and contraction of host materials due to lithium intercalation, solid electrolyte interface (SEI) growth and binder swelling.

This phenomenon of pouch cell "swelling" is typically addressed by one of the following approaches:

- Firstly, by fixed displacement, where the cell is dimensionally constrained.
- Secondly, by a force proportional to displacement, most typically through the action of a spring. This deployment is most common in the laboratory environment during single cell cycling and abuse testing.

- Thirdly, by leaving the cell unrestrained, where the cell is not provided with any support.

Production battery modules are typically provided with a fixed displacement. The dimension can be set to either apply a pre-load the battery stack or can be over-sized, allowing the expanding cells to fill the space. In both cases, once the dimensional limits are reached, additional stress will develop as the cells swell. More often than not, the cell stack also contains compliant materials in between the cells, thereby adding some proportional force and allowing some cell swelling before additional stresses are experienced.

The concern with testing an unconstrained cell, either during cycling or abuse, is that it does not reflect reality and may lead to behavior, particularly failure pathways, that are artificial. For example, abuse testing of an unconstrained pouch cell may lead to severe ballooning and failure in a location other than at the tabs or pouch seams, where failures would be expected.

The relationship between cell swelling and performance is reciprocal. Firstly, it is known that both the vigor of the cycling as well as the age of the cell can impact the stress developed in a cell. Secondly, the extent of externally applied pressure or force can affect the rate of cell ageing. Although by no means comprehensive, Table 1 highlights some tests where external pressures were studied, and specifically whether a fixed force or displacement was applied.

Some of the general observations made in the above publications include:

- *"Dynamic pressure generated during discharging/charging which looks like "cell breathing".*
- Cell pressure increases with state-of-change (SOC) and cycle number.
- Unconstrained cells fade or age quicker.
- Spring supported cells (proportional force) faded slower when compared to fixed displacement.
- *"The spring constraint scheme can maximize the positive effect of external pressure on lithium-ion batteries by maintaining a relatively stable external pressure".*
- Zero pressure led to fastest capacity fade: lower fade seen for supporting higher pressures.
- *"An optimum pressure around 1.3 MPa is shown to be beneficial to reduce cyclable-lithium loss during cycling"*

In general, it would appear that some pressure is beneficial for cell ageing and that no or low pressure tended to accelerate capacity fade. It should be noted that this review ignored the impact of cell temperatures and charge rates which are both critical contributing factors for cell ageing. This paper explored the stress developed as a consequence of cycling and particularly abuse, which is a gravely underexplored area.

Experimental Setup

Battery cell

A commercial LG Chem E65D rechargeable lithium ion pouch cell with NMC chemistry was selected for this study. Key specifications are given in Table 2:

Considering the cell capacity, the standard C-rates for change and discharge are both C/3. The cell specification sheet further provides expectations for thickness increase between beginning- and end-of-life, acknowledging that swelling of the cells are expected as they age. The cell specification sheet further calls out an "*Initial Pressure*" of greater than 30 kilograms and requires that the "*ell must be pressurized during lifetime*" with "*Pressure force direction : perpendicular to Cell body surface (whole area)*". Moreover that "*If the cell is not pressurized properly during lifetime, the performance and life cannot be guaranteed*".

TABLE 1 Relationship between pressure and cell performance.

	Zhang et al. [1]	Zhang et al. [2]	Barai et al. [3]	Barai et al. [4]	Zhou et al. [5]	Mussa et al. [6]
Chemistry	LiFPO6	-	NMC	NMC	NMC	-
Capacity (Ah)	37 Ah	5.3	25	15	26	0.5
Dimensions (mm)	269 212 7.4	245 120 4.86	-	186 165 56	227 161 7.45	25 35 6.5
Pressure (bar)	-	0.69	0 0.2 0.4 0.8	0 0.3 1	0 10	1 10
Fixed	Displacement	Displacement	Force	Force	Force	Displacement
C-rates	0.5	0.5 1 3	-	1	1/3	½

TABLE 2 E65D key specifications.

Property	Value	Unit
Nominal capacity	66.0	Ah
Thickness	11.5	mm
Width	159	mm
Height (without tabs)	290.5	mm
Nominal Voltage	3.66	V
Operating Voltage	2.5 to 4.2	V
Standard Charge - Constant current	21.7	A
Standard Charge - Constant voltage	4.2	V
Standard Discharge - Constant current	21.7	A
Standard Discharge - End voltage (cut-off)	2.5	V

FIGURE 1 Load measurement fixture.

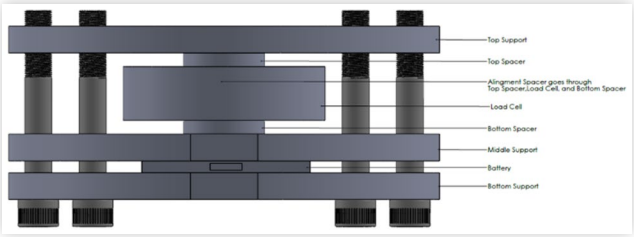

Load measurement

To enable both the initial load application and measurement of the force exerted by the cell during cycling and abuse testing, a load measurement fixture was designed and built. As shown in Figure 1, the pouch cell was placed in between two aluminum plates (the bottom and middle support). The forces exerted by the cell were evenly distributed along the middle support and were recorded by a Honeywell Model 73 low profile load cell connected to an MTS 458.10 MicroConsole amplifier. Static compression elements (bolts, nuts and top support) set the initial compressive load. Note that the final test configuration was inverted to reduce the weight above the battery cell and thereby reduce the pre-loading.

One side of the middle support facing the battery cell was milled to create grooves to accept seven (7) K-type thermocouples (TC), with locations outlined in Figure 2. Thermocouples were installed in such a way to avoid stress points and not damage the cell under compression. This was done in part to avoid the compromised results as reported by Cannarella and Arnold [7]. TC1 and TC2 were placed near the positive and negative tabs respectively, TC3 at the center of the cell, TC4 and TC6 midpoint along the length. TC5 and TC7 were on either side of TC3 in the width direction. An additional thermocouple, indicated as "PEC", was placed close to the center as safety indication to the cycler.

FIGURE 2 Thermocouple locations on the cell.

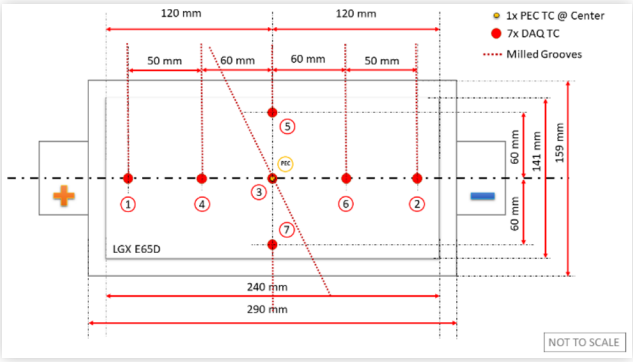

Cycling

To enable cycling, a new cell was connected to a PEC model ACT 0550 cycler and subjected to the following C/3 CC-CV charge cycle:

- Constant Current (CC) = 21.7 A
- Constant Voltage (CV) = 4.2 V

The discharge current was also C/3 with a cut-off voltage of 2.5 V.

One-hour rest periods were introduced between every charge and discharge step and tests were carried out in laboratory ambient temperatures of approximately 20 °C.

The installation of the cell in the fixture is shown in Figure 3 and shows current lines in heavy wires bolted to the tab busbar, as well as thin voltage sense wires connected with alligator clamps.

For cycling, the cell was installed at an initial SOC of approximately 25% SOC which corresponds to a voltage of 3.57 V, and preloaded to 294 N (0.063 bar) with corresponded to the 30 kilograms suggested by the cell

FIGURE 3 Load measurement during cycling.

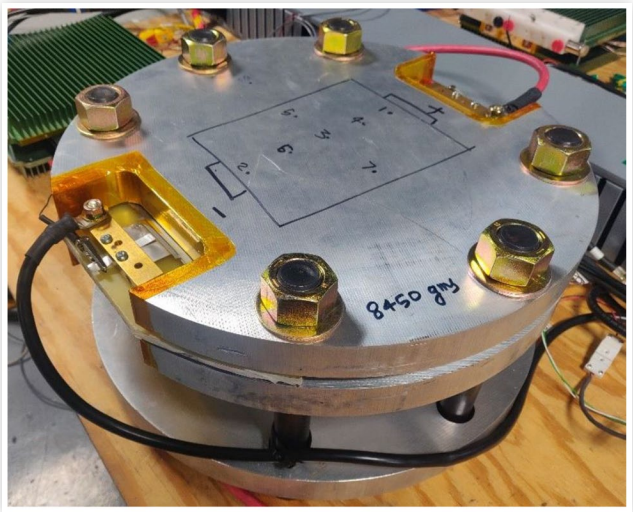

specification sheet. This was accomplished by tightening the six nuts in a uniform manner.

Current, voltage, force and temperatures were continuously recorded at a rate of 1 Hz for the duration of the test.

Short Circuit

The preloading of the battery cell was done in a similar manner as that of the cycling with the big difference that the cell was charged to 100% SOC prior to commencement of the test.

For the short circuit test, the load measurement fixture was placed inside a blast chamber, shown in Figure 4 below, before installation of top of the fixture or the chamber door. The picture also shows the spark ignition system on the left, intended to ignite any escaping vapors, video camera and battery cell. Not shown is an extraction system connected to an exhaust scrubber.

FIGURE 4 Placement of the load measurement assembly inside the blast chamber for the short circuit test.

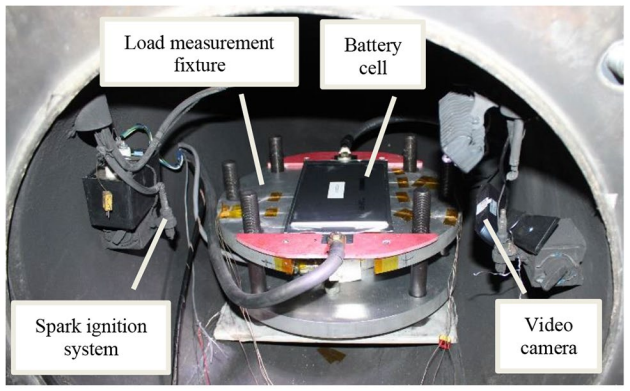

The short-circuit abuse tests conducted in this study adhered to the guidelines outlined in SAE J2464 [9]. To facilitate this testing, a customized short circuit rig was employed, which was specifically designed to create an external hard short resistance of 2 mΩ between positive and negative tabs of the cell by means of a pneumatically actuated rapid contactor. The short circuit current was measured using a LEM LF1010-S current transducer with a measuring range of 2700 A, but was used for reference only.

Data and images were synchronized with time zero corresponding to the initiation of the short circuit and all the channels (current, voltage, force and temperatures) were recorded at a rate of 10 Hz. Video images were taken at 60 frames per second with two camera angles provided.

Results

Cycling Testing

Figure 5 shows the details of a single charge-discharge cycle. For brevity, only TC1 is shown and positive currents

FIGURE 5 Voltage, load, temperature and current development during a typical cycle.

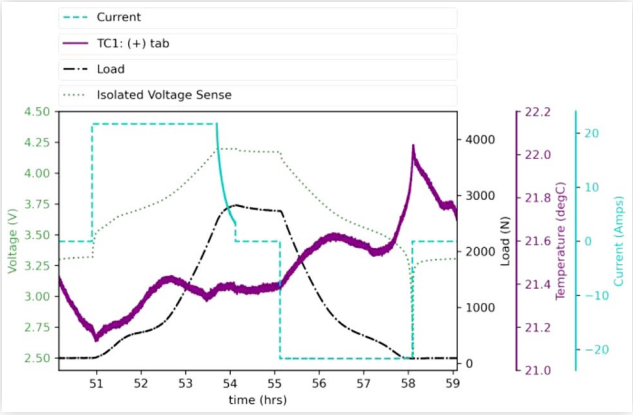

are associated with charging. The following features can be distinguished:

- Hour 51: CC charge leading to increase in voltage, cell temperature and load.
- Hour 53.5: CV charge with decreasing current, increasing load and near constant voltage and temperature.
- Hour 54: One hour rest with zero current during which the temperature stays near constant and voltage and load appears to trail off.
- Hour 55: CC discharge with decreasing voltage and load and increasing temperature.
- Hour 57.5: Continuation of the CC discharge with rapid voltage decrease to minimum voltage and associated temperature increase.
- Hour 58: One hour rest with zero current, decreasing temperature and near-constant load and voltage.

The cycling test spanned a total of 14 days, with a distinctive approach to assessing stress generation. During the first seven days, the pouch cell underwent 20 cycles according to the procedure described earlier. Cycling was temporarily halted for two days (hour 168 to 220) at a 30% SOC, corresponding to 3.606 V. The cessation and resumption of cycling were introduced to study the effect of an interrupted routine on stress generation within the pouch cell. A second phase of cycling followed, but was terminated after five days as loads persisted above a 4,000 N (0.87 bar) threshold, signaling the necessity for intervention to avoid possible cell damage or failure.

Figure 6 provides a comprehensive representation of the load measurements obtained during the cycling test. The initial peak load in the cycling routine occurred just below 2,000 N (0.43 bar), immediately after the commencement of the constant voltage region of the Constant Current Constant Voltage (CCCV) charging phase. Note that the calculated pressure is based on measured force and cell dimensions. The peak load displayed a consistent upward trend throughout the initial

FIGURE 6 Voltage and load as a function of time.

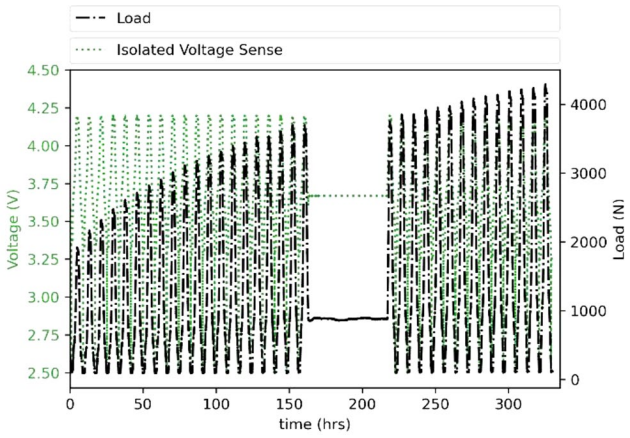

20 cycles, reaching an approximate value of 3,800 N (0.82 bar). After pausing the cycling for two days, the experiment was resumed to assess whether the generated stress would be relieved as a result of the rest period. However, it was observed that the very first peak load measured, immediately following the resumption of cycling, remained near the last recorded peak from the initial seven days of cycling. The test continued for an additional 14 cycles, during which the peak load exceeded 4,200 N (0.91 bar).

The load associated with 30% SOC similarly increased with each cycle, ranging from about 330 N (0.07 bar) to about 590 N (0.13 bar) between the first and last cycle, whereas the load at the cut-off voltage of 2.5 V remained constant throughout the test at a value of approximately 80 N (0.02 bar), which corresponded to the mass of the top support. This suggested that the cell had unloaded to a point where the fixture bolts were no longer constraining the cell.

Figure 7 shows the variation in temperatures, revealing a typical diurnal cycle. The extent of these cell temperature variations – in the order of 4 °C – were

FIGURE 7 Voltage and temperatures as a function of time.

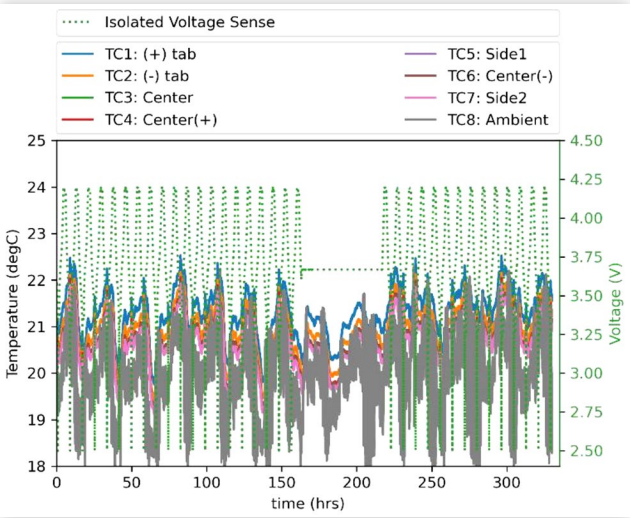

FIGURE 8 Hysteretic loop for the load measurement during cycling.

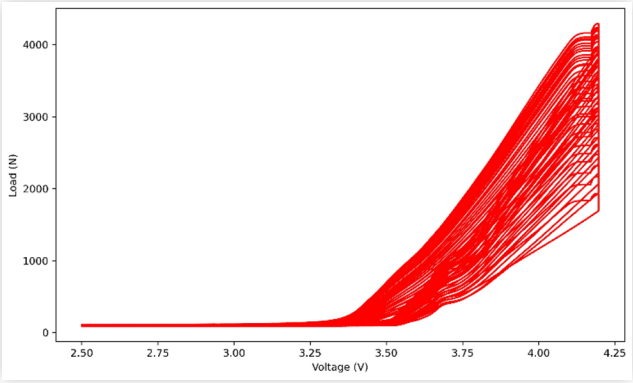

much bigger than the temperature range of less than 1 °C observed in Figure 5, suggesting the Ohmic heating was secondary to ambient temperature impacts. The relatively large thermal mass of the plate with the embedded thermocouples no doubt contributed to the result.

Figure 8 presents the same load data from Figure 6 but in a continuous hysteretic loop format. Notably, the data reveals a consistent trend of increasing peak loads for each cycle within the 14-day experimental period. During the resting period following cell discharge, the stress generation reverted to the preloaded condition. This phenomenon underscores the pouch cell's hysteretic behavior, attributed to its degradation or aging, and offers valuable insights into its mechanical characteristics under cyclic stress.

Short Circuit Testing

Two short circuit tests were performed, in each case using a new cell and charging it to 100% SOC prior to installation.

Test 1 Figure 9 presents stress generation data for the first two minutes following the application of a short trigger at time zero. Within seconds, a peak load of approximately 800 N (0.17 bar) was recorded. Despite adhering to the J2464 test standard's one-hour monitoring requirement, the load remained at 200 N (0.04 bar), falling below the initial preload within the first two minutes. Voltage dropped to about 2 V immediately after the short circuit and down to zero in concert with the maximum load.

Figure 10 shows temperature data for Test 1, revealing that the highest temperatures registered remained below 30 °C. The application of a hard external short resulted in a peak current value of approximately 1900 A, which rapidly decreased to zero within ten seconds. Simultaneously, the voltage dropped from 4.2 V - representing the preconditioned state of the cell at 100% SOC - to 0 V.

FIGURE 9 Voltage and load during the Test 1.

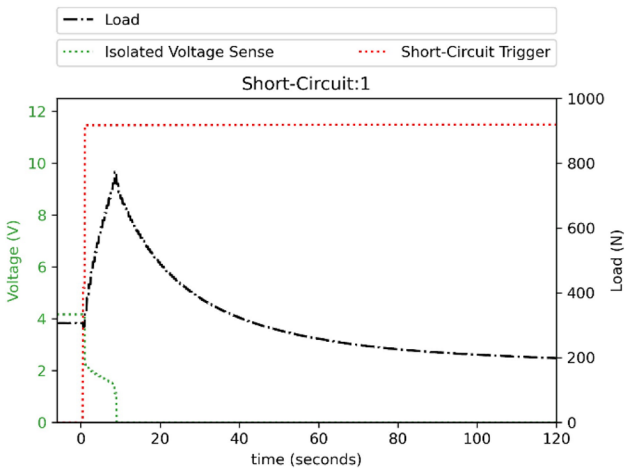

FIGURE 10 Voltage, temperatures and current during the Test 1.

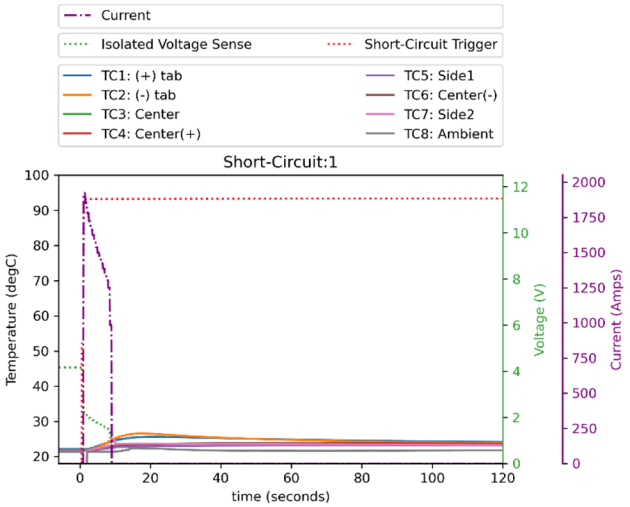

A review of selected frames from the video imaging in Figure 11 shows escaping vapors at approximately three seconds at the negative tab location, presumably the electrolyte, with the emergence of flames in the same location a second later. At about six seconds, fire also appeared at the positive tab but all flames were extinguished after about 10 seconds.

As seen in Figure 12, inspection of the cell after the test revealed that the tab had torn off, presumably during the release of the electrolyte, combined with the strain placed on the tab by the busbar connected to the current cable.

This no doubt explained the sudden drop in current at about 10 seconds and also the absence of significant load or temperature increase beyond that time due to the absence of an external short. This observation served as the motivation for conducting a second test. The torn tab did not however explain the presence of flames in the vicinity of both tabs during those first 10 seconds.

FIGURE 11 Images corresponding (from top to bottom) to electrolyte release (3 seconds), fire at negative tab (4 seconds), fire at the positive tab (6 seconds) and end of all fires (10 seconds) for Test 1. Timestamps are in MM:SS:FRAME.

Test 2 For the second test, the current cable connections were modified to reduce strain on the tab by affixing the cable lug to a non-conductive bridge. Figure 13 compares the cell tab electrical connections for the two tests.

Figure 14 shows the voltage and load with an immediate drop of the former from about 4.2 V to about 1 V after the short circuit and a further gradual reduction to

FIGURE 12 View of the torn tab after the Test 1.

FIGURE 13 Comparison of the electrical connections.

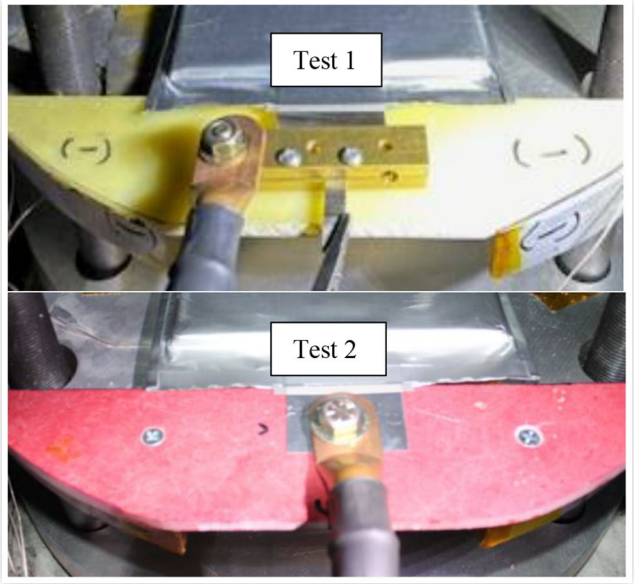

FIGURE 14 Voltage and load during the Test 2.

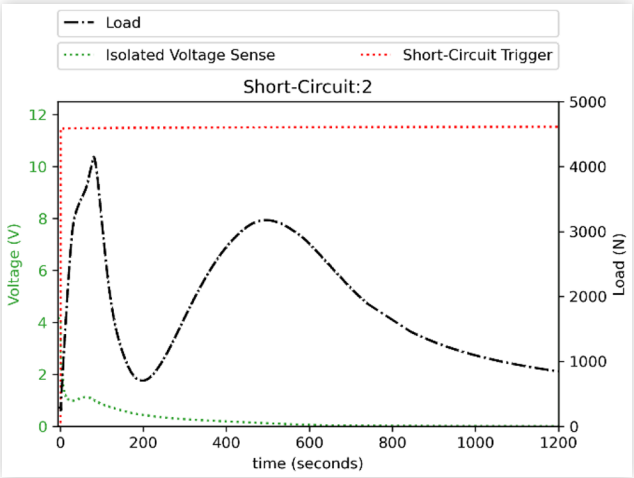

zero after approximately 600 seconds. It also illustrates the stress generation with two distinct load peaks. The first peak occurred at approximately 90 seconds, registering a value of around 4,200 N (0.91 bar). The second peak occurred around 510 seconds, exhibiting a value of approximately 3,200 N (0.69 bar). Between these two load peaks, the load momentarily decreased to approximately 600 N (0.13 bar) at 200 seconds before beginning to rise again. After the second peak, the load gradually dropped to below 900 N (0.19 bar) after about 20 minutes of initiation of the short circuit. The first peak was likely due to the boiling of the electrolyte whilst the second was likely related to thermal expansion of the cell components during subsequent heating.

The corresponding temperatures in Figure 15 peaked at about 50 °C with the maximum current again approaching 2000 A. The current is however sustained for much longer, eventually dropping to zero only after more than 600 seconds. Is it also notable that the ambient temperature (TC8) measured inside the blast chamber was increasing all the time, approaching 30 °C by the end of the test. In the absence of other heat sources, this was in response to the heating of the cell and the fixture due to the sustained short circuit.

Selected frames from the video imaging in Figure 16 shows escaping vapors at ~90 seconds but no further evidence that the peak load was achieved. Similarly at 510 seconds, there is nothing to indicate the presence of the second load peak, and by this time much of the vapors had cleared. Notably, no flames were visible during the second test. The pouch cell, under forced abuse conditions resulting from an external short, vented from sites near the positive and negative tabs, with boiling electrolyte observed at the tabs in the video feed.

Test Comparison A comparison between the two short circuit tests is offered in Table 3 below. Test 1 exhibited lower loads and temperatures without any voltage loss and limited mass loss, all of which support the notion that

FIGURE 15 Voltage, temperatures and current during Test 2.

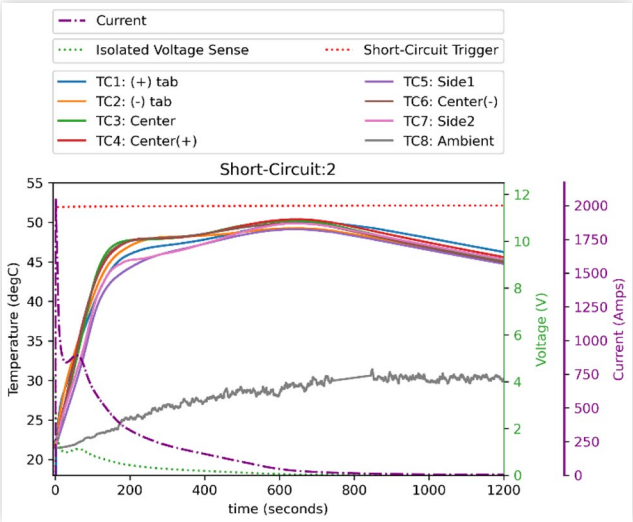

FIGURE 16 Images corresponding to maximum load (90 seconds, top) and second load peak (510 seconds, bottom) for Test 2. Timestamps are in MM:SS:FRAME.

TABLE 3 Short circuit test comparisons.

Feature	Test 1	Test 2
Maximum load (N) at time (seconds)	~800 @ 10	~4000 at 90
Maximum pressure (bar)	0.17	0.87
Maximum temperature (°C) at time (seconds)	28 at 15	~50 at 600
Final load (N) at time (seconds)	~200 at 120	~900 at 1200
Final pressure (bar)	0.04	0.19
Voltage before test (V)	4.101	4.165
Voltage after test (V)	4.101	1.465
Voltage loss (V)	0	2.7
Mass before test (g)	1000.6	1002.2
Mass after test (g)	996.6	973.8
Mass loss (g)	4.0	28.4

the short circuit was interrupted by the tearing of the tab and that the cell was not fully stressed. By comparison, Test 2 experienced a measurable mass loss due to persistent venting of the electrolyte and significant voltage drop. It should be noted that the voltages are open circuit measurements after extracting the cell from the test fixture, hence the apparent recovery of voltage for the second test that had previously measured zero in the fixture.

Discussion

This study investigated stress generation within large pouch cells, focusing on their behavior under cycling and abuse conditions.

In cycling tests, the experiment illuminated the pouch cell's response to repeated charge and discharge cycles, uncovering a persistent increase in peak load throughout the initial 20 cycles of the routine. This intriguing trend continued until 34 cycles were completed, after a brief halt and resumption of cycling, signifying the cell's ability to maintain ageing-induced stress patterns. Moreover, the cyclic behavior displayed by the pouch cell, wherein stress generation consistently returned to preloaded conditions after rest periods, underscored the cell's hysteretic response, indicative of aging and degradation.

Moving to the short circuit tests, these investigations vividly portrayed the pouch cell's behavior under forced abuse conditions. Test 1 was interrupted by the tearing of a tab and disruption of the short circuit, but did reveal intriguing yet short lived flames at the tab locations. In test 2, the pouch cell exhibited a different response, with two distinct load peaks observed, along with notable thermal and voltage behavior. Importantly, venting was observed, showcasing the cell's response to external short circuit abuse. The peak load measured during abuse was not much different from that seen after on 14 days of cycling.

Recommendations

This study did not consider the impact of variations in pre-loading on the stress development during cycling, nor the effect of more aggressive C-rates. The cycling programming also did not evaluate the capacity difference or other measure of ageing as a result of the cycling and hence did not attempt to correlate the stress levels with that of ageing. All three aspects should be considered for future study.

For the abuse testing, other than ensuring proper cell fixturing, different cell abuse methods, such as overcharge or nail penetration, can be considered to augment the short circuit test results.

References

1. Zhang J., "Effects of Pressure Evolution on the Decrease in the Capacity of Lithium-Ion Batteries," *Int. J. Electrochem. Sci.*, pp. 8422-8436, Sep. 2020, doi:10.20964/2020.09.71.
2. Zhang, Y.C., Briat, O., Deletage, J.-Y., Martin, C. et al., "Characterization of External Pressure Effects on Lithium-Ion Pouch Cell," in: , *2018 IEEE International Conference on Industrial Technology (ICIT)*, (Lyon: IEEE, Feb. 2018), 2055-2059, doi:10.1109/ICIT.2018.8352505.

3. Barai, A., Guo, Y., McGordon, A., and Jennings, P., "A Study of the Effects of External Pressure on the Electrical Performance of a Lithium-Ion Pouch Cell," in: , *2013 International Conference on Connected Vehicles and Expo (ICCVE)*, (Las Vegas NV, USA: IEEE, Dec. 2013), 295-299, doi:10.1109/ICCVE.2013.6799809.
4. Barai A. et al., "The Effect of External Compressive Loads on the Cycle Lifetime of Lithium-Ion Pouch Cells," *Journal of Energy Storage*, vol. 13, pp. 211-219, Oct. 2017, doi:10.1016/j.est.2017.07.021.
5. Zhou L. et al., "A Study of External Surface Pressure Effects on the Properties for Lithium-Ion Pouch Cells," *Int J Energy Res*, vol. 44, no. 8, pp. 6778-6791, Jun. 2020, doi:10.1002/er.5415.
6. Mussa A.S., Klett M., Lindbergh G., and Lindström R.W., "Effects of External Pressure on the Performance and Ageing of Single-Layer Lithium-Ion Pouch Cells," *Journal of Power Sources*, vol. 385, pp. 18-26, May 2018, doi:10.1016/j.jpowsour.2018.03.020.
7. Cannarella J. and Arnold C.B., "Stress Evolution and Capacity Fade in Constrained Lithium-Ion Pouch Cells," *Journal of Power Sources*, vol. 245, pp. 745-751, Jan. 2014, doi:10.1016/j.jpowsour.2013.06.165.
8. Fuchs, G., Willenberg, L., Ringbeck, F., and Sauer, D.U., "Post-Mortem Analysis of Inhomogeneous Induced Pressure on Commercial Lithium-Ion Pouch Cells and their Effects," *Sustainability* 11, no. 23 (2019): 6738, doi:10.3390/su11236738.
9. Battery Safety Standards Committee, "Electric and Hybrid Electric Vehicle Rechargeable Energy Storage System (RESS) Safety and Abuse Testing," *SAE International.*, doi:10.4271/J2464_202108.

Contact Information

The author can be contacted at andre.swarts@swri.org.

Acknowledgments

The authors wish to acknowledge funding by the SwRI Advisory Committee for Research as well as Fassett Hickey and Michael Huebenthal Jr from SwRI for assistance with the design, manufacture and calibration of the load measurement fixture.

Definitions/Abbreviations

CC - Constant Current
CV - Constant Voltage
OCV - Open Circuit Voltage
SEI - Solid Electrolyte Interface
SOC - State of Charge
TC - Thermocouple

ISSN 0148-7191